Journal of Power Sources 516 (2021) 230700

Contents lists available at ScienceDirect

Journal of Power Sources

journal homepage: www.elsevier.com/locate/jpowsour

On the rate capability of supercapacitors characterized by a constant-phase element

Gibson P. Scisco [a,*], Mark E. Orazem [b], Kirk J. Ziegler [b], Kevin S. Jones [a]

[a] Department of Materials Science and Engineering, University of Florida, 32611, Gainesville, FL, USA
[b] Department of Chemical Engineering, University of Florida, 32611, Gainesville, FL, USA

HIGHLIGHTS

- Capacitance of electrochemical capacitors exhibits a power law with test rate.
- Constant phase element behavior of electrochemical capacitors is responsible.
- Constant phase element parameters can be determined from multiple methods.
- These parameters can be used to estimate the rate capability of capacitors.

ARTICLE INFO

Keywords:
Constant phase element
Electrochemical impedance spectroscopy
Supercapacitor
Cyclic voltammetry

ABSTRACT

The capacitances of electrochemical systems determined from cyclic voltammetry (CV) are difficult to compare due to the unavoidable constant-phase element (CPE) behavior of such systems. These difficulties can be illustrated by simulated voltammograms of simplified circuits composed of a resistor in series with a CPE (R-CPE circuits). The capacitance extracted from CV of R-CPE circuits follows a power law relationship with sweep rate. By comparing the CV-obtained capacitance with that obtained from electrochemical impedance spectroscopy (EIS) data, a critical sweep rate can be defined as the rate where these capacitances intersect. This critical rate can be used to formulate an effective time constant for R-CPE circuits. Sweep rates at least two orders of magnitude below the critical rate should be used in CV to mitigate the influence of the system's time constant on the measured capacitance. To allow for more accurate comparisons of supercapacitors, the CPE parameters R, Q, and α should be reported, rather than the capacitance vs. sweep rate data from CV measurements.

1. Introduction

Electrochemical double layer capacitors (EDLCs), also known as supercapacitors, are an energy storage technology with attractive power performance and long-term cycle stability [1]. There is ongoing discussion regarding the proper methods of measuring and reporting the performance of supercapacitor devices [2–4]. The most important performance metric of a supercapacitor is its capacitance. The capacitance cannot be measured directly, so it must be calculated based on measurements of current, charge, and voltage [5,6]. Capacitance is expected to be a thermodynamic property and therefore constant for a given system, however, the capacitance calculated from electrochemical measurements, referred to hereafter as the "effective capacitance," is known to be a function of the sweep rate in the case of CV or the current density in the case of galvanostatic measurements [7]. In EIS analysis, it is common to calculate the capacitance from the imaginary impedance as $C_{EIS} = (-\omega Z_j)^{-1}$ [4,8], however, this relationship also gives a frequency-dependent value of capacitance. The evolution of the effective capacitance with charge rate is termed the rate capability of the capacitor and is another important metric for determining the application of a supercapacitor. However, differences in test methodologies make drawing informed comparisons between EDLCs reported in the literature difficult. It would therefore be preferable to report rate-invariant metrics rather than disparate values of effective capacitance at various charging rates. Methods for predicting the rate performance of supercapacitors based on easily obtainable, rate-invariant

* Corresponding author. Department of Materials Science and Engineering, University of Florida, 549 Gale Lemerand Drive, PO BOX 116400, Gainesville, Fl, 32611, USA.
E-mail address: gpscisco@umd.edu (G.P. Scisco).

https://doi.org/10.1016/j.jpowsour.2021.230700
Received 3 June 2021; Received in revised form 8 October 2021; Accepted 25 October 2021
Available online 30 October 2021
0378-7753/

metrics can facilitate faster testing procedures and more accurate comparisons between devices.

The variation in effective capacitance as a function of charging rate has been attributed to constant-phase element (CPE) behavior [7], and EDLCs can be reasonably well-modeled as a circuit composed of a resistor and CPE in series (R-CPE circuit). CPEs have been studied extensively through electrochemical impedance spectroscopy (EIS). The impedance of an R-CPE circuit is defined as

$$Z = R + \frac{1}{(j\omega)^{\alpha} Q} \tag{1}$$

where Q is the CPE coefficient and α is the dispersion coefficient. Q has the derived units of F $s^{\alpha-1}$, and the dispersion coefficient α is a unitless number $0 < \alpha \leq 1$, with $\alpha = 1$ being equivalent to ideal capacitive behavior. An equation for the current passing through an R-CPE circuit during a voltage sweep has been derived by Allagui et al. [9] as

$$i(t) = Q\frac{V_f - V_i}{t_f - t_i}\left[\frac{t^{1-\alpha}}{\Gamma(2-\alpha)} - \frac{(RQ)t^{1-2\alpha}}{\Gamma(2-2\alpha)} + \ldots\right] \tag{2}$$

where V_f and V_i are the final and initial voltages, and Γ(x) is the gamma function.

Brug et al. derived the equation [10].

$$C_B = Q^{\frac{1}{\alpha}} R^{\frac{1-\alpha}{\alpha}} \tag{3}$$

to convert the CPE parameters to units of capacitance. Eq. (3) was derived under the assumption that the observed frequency dispersion of the CPE was due to a distribution of time constants across the electrode surface. This equation gives a single, rate-invariant value of capacitance for the R-CPE system. In CV testing, the effective capacitance can be calculated from

$$C_{CV} = \frac{\int_{Vi}^{Vf} i(V)dV}{\nu\left(V_f - V_i\right)} \tag{4}$$

based on the total charge stored on the capacitor. Allagui et al. published equations for calculating the effective capacitance of an R-CPE circuit based on its charging rate [9]. The authors derived equations both for galvanostatic charge-discharge and CV based on a fractional derivative approach expanding on the work of Montella and Westerlund [11,12] to calculate the capacitance based on the charge rate and the CPE parameters. Their relation for CV analysis is given by

$$C_A = \frac{Q}{\Gamma(3-\alpha)}\left(\frac{\nu}{\Delta V}\right)^{\alpha-1} \tag{5}$$

where Q and α are the CPE parameters, ν is the sweep rate, and ΔV is the voltage window. Eqs. (4) and (5) should be equal, but as will be discussed later, this is not always the case.

In the present work, the capacitance calculated from Eqs. (4) and (5) is compared directly to the capacitance calculated from the Brug formula, Eq. (2), for both simulated and experimental supercapacitors. The intersection between the calculated capacitances is used to derive a critical CV sweep rate for an R-CPE system. The results demonstrate the difficulty in obtaining accurate resistance values from CV and provide additional support for the argument that CPE behavior of EDLCs arises from surface distributions of time constants. Lastly, a case is made for reporting CPE parameters of EDLCs as a way to more easily compare their performance.

2. Methods

Simulations were performed using R software. Voltammograms of simulated circuits were calculated using Eq. (2), and the capacitance was calculated from Eq. (4) with 1000 time steps using the trapezoidal rule. To account for current from Eq. (2) approaching -∞ at t = 0, the first time step was removed from the data for calculating capacitance. This allowed for a more accurate depiction of the critical rate of the R-CPE circuit. Since Eq. (2) is symmetric in the forward and reverse scans, only the forward scan was used to calculate the capacitance.

The construction of the CNT-based capacitors has been described elsewhere [13]. Briefly, anodized aluminum oxide (AAO) templates were made using a two-step anodization. The templates were then coated with carbon to form carbon nanotubes (CNTs) via chemical vapor deposition (CVD). Electrodes formed in this way were assembled in a pouch-cell capacitor configuration within a dry Ar glovebox before introducing the solvent-free ionic liquid electrolyte (1-ethyl-3--methylimidazolium tetrafluoroborate, EMIM-BF4, Iolitec). Once sealed, the cells were removed from the glovebox for testing.

Electrochemical testing was performed on a Versastat 3 potentiostat (Princeton Applied Research). For CV, sweep rates were 10, 50, 100, and 500 mV s^{-1} on the voltage range of 0–1 V or −0.1 – 1 V. Differences in voltage ranges between devices were accounted for in the calculations. Three scans were performed at each sweep rate and the third was used for analysis. The same devices were tested using EIS on the frequency range 10^5–10^{-1} Hz with a signal amplitude of 10 mV. To calculate the CPE parameters from EIS, the low-frequency region <25 Hz was fitted using an R-CPE circuit. EIS data was fitted using the measurement model software [14].

3. Results and discussion

The time-domain response of an ideal R-C circuit can be written as

$$i(t) = \nu C\left[1 - \exp\left(-\frac{t}{RC}\right)\right] \tag{6}$$

where ν is the sweep rate [15]. Voltammograms simulated from Eqs. (2) and (6), shown in Fig. 1, exemplify the important differences between the R-CPE (red) and R-C (black) circuits.

The currents of the two circuits are not greatly different, as can be seen in Fig. 1a. This current can be used to calculate capacitance through

$$i = \nu C \tag{7}$$

where i is the current and ν is the sweep rate [16].

When Eq. (7) is applied to normalize the current, as in Fig. 1b, the differences between the R-C and R-CPE circuits become clearer. For the ideal case, the capacitance reaches a steady-state value after a short time, based on the time constant of the circuit, and the curves overlap for each scan rate. For the R-CPE circuit, the i/ν curves show a monotonic increase with decreasing scan rate. Eq. (7) can also be used to calculate capacitance by fitting the line produced by plotting the capacitive current against sweep rate. Gharbi et al. compared the value of C_A calculated using CPE parameters obtained from EIS to the value of capacitance calculated from the slope of Eq. (7) and found that a constant value of capacitance cannot be obtained when the system behaves as a CPE [17]. Those authors also pointed out the importance of scan rate selection for CV measurements of capacitance, and again raised the possibility of CPE behavior originating from surface distributions of time constants as proposed by Brug et al. [10]. The simulated R-CPE circuits in the present work are able to recreate Gharbi's experimental result, as shown in Fig. 2a. The current of the R-CPE circuit does not follow a linear trend with sweep rate; therefore, the capacitance cannot be estimated from the slope. Plotting the data on a log-log scale, as in Fig. 2b, shows that the current of the R-CPE follows a power law with sweep rate based on the value of α, as has been previously reported [7]. However, the pre-exponential term of this relationship has not been discussed. Based on the simulations, the complete power law fitting has been found to be

$$i\left(V_f\right) = \frac{Q}{\Gamma(2-\alpha)\Delta V^{\alpha-1}}\nu^{\alpha} \tag{8}$$

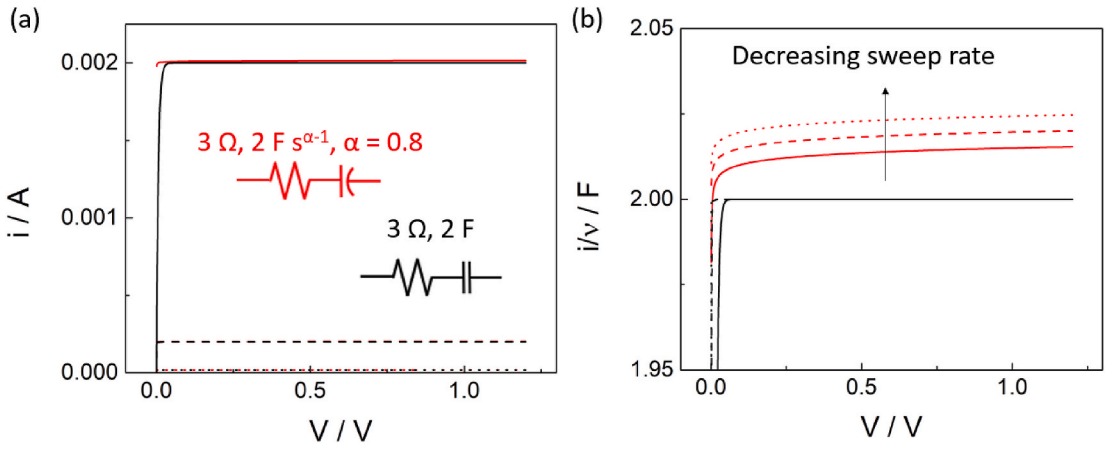

Fig. 1. Simulated voltammograms based on the R-CPE circuit (red) and the R-C circuit (black) for sweep rates of 10^{-5} (dotted), 10^{-4} (dashed), and 10^{-3} (solid) V s^{-1}. The un-normalized current (a) doesn't show an obvious difference between the two systems at low rates, but by normalizing to the sweep rate (b), the non-limiting behavior of the CPE circuit becomes clear. Since the CPE circuit never reaches a steady-state value of double-layer charging current, the calculated capacitance does not approach a limiting value. (For interpretation of the references to colour in this figure legend, the reader is referred to the Web version of this article.)

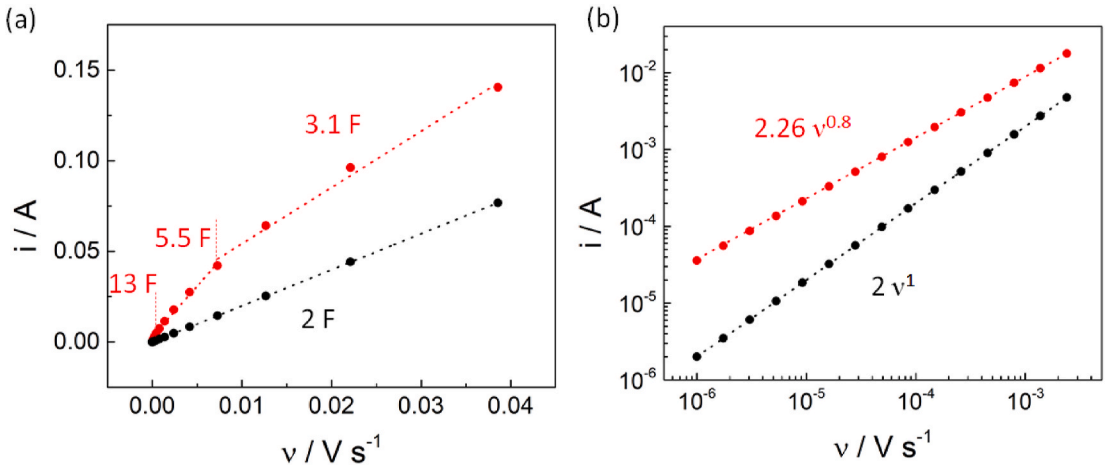

Fig. 2. Calculating capacitance from the slope of the current vs. sweep rate curves of the simulated circuits shows that (a) the R-CPE current cannot be modeled as a linear function of sweep rate as in Eq. (7). The slope of different line segments is shown as varying values of capacitance above the segments. Replotting the same data on a log-log scale (b) shows that the current of the R-CPE follows a power law whose slope is based on the value of α. The circuits here are the same as depicted in Fig. 1a. For each data point, the current at the final voltage, 1.2 V, was used.

meaning that the pre-exponential term can be directly related to the value of the CPE parameter Q. Eq. (8) was found to hold only at low sweep rates. Importantly, the value of the resistance does not influence the current at these low rates. This power law effect indicates that the calculated capacitance from Eq. (7) will never reach a stable value, even at very low scan rates [18].

Similar relationships between current and sweep rate have been used in pseudocapacitive research by using

$$i(V) = k_1\nu + k_2\nu^{\frac{1}{2}} \tag{9}$$

to determine the relative contributions of surface capacitive ($k_1\nu$) and diffusive ($k_2\nu^{1/2}$) current at a particular potential [19]. This analysis glosses over the CPE behavior of the electrode by assuming that the current can be described as a superposition of ideally capacitive ($\alpha = 1$) and ideally diffusive ($\alpha = 0.5$) currents, neither of which are true. When Eq. (9) is applied to the R-CPE data presented in Fig. 2, there is no linear region in a plot of $i/\nu^{1/2}$ as a function of $\nu^{1/2}$. Restricting the analysis to sweep rates above 1 mV s^{-1}, more commonly used experimentally, a quasi-linear region can be fitted to obtain $k_1 = 2.4$ and $k_2 = 0.28$, suggesting that some amount of the current is due to diffusive effects, when in fact the entire current response is from resistive and constant-phase elements. The analysis using Eq. (9) over a truncated range of sweep rates might be used to suggest that CPE behavior originates from diffusive effects, but since the full sweep rate range cannot be fitted well by Eq. (9), this conclusion is erroneous.

The effective capacitance calculated from Eq. (4) can also be plotted against sweep rate with similar results. R-CPE circuits simulated using Eq. (2) and their corresponding effective capacitances are shown as a function of sweep rate in Fig. 3. Two distinct regimes are visible, distinguished by a critical rate. Below this critical rate, the effective capacitance exactly follows a power law with sweep rate as in Eq. (5), but above the critical rate, the system exhibits resistive behavior. The switch from capacitive to resistive behavior results in an effective capacitance far below the expected value.

The power law dependence of the current of a CPE has been pointed out previously by Sadkowski [7] and related to the dispersion coefficient of the CPE, but the pre-exponential term has previously been ignored. When the test rate approaches the critical rate, the power law behavior is skewed by the influence of the finite time constant of the system, and the calculated capacitance is lower than that predicted by Eq. (5). Larger time constants, either from larger resistances or capacitances, lead to more sluggish behavior at the switching potentials that can lead to "leaf

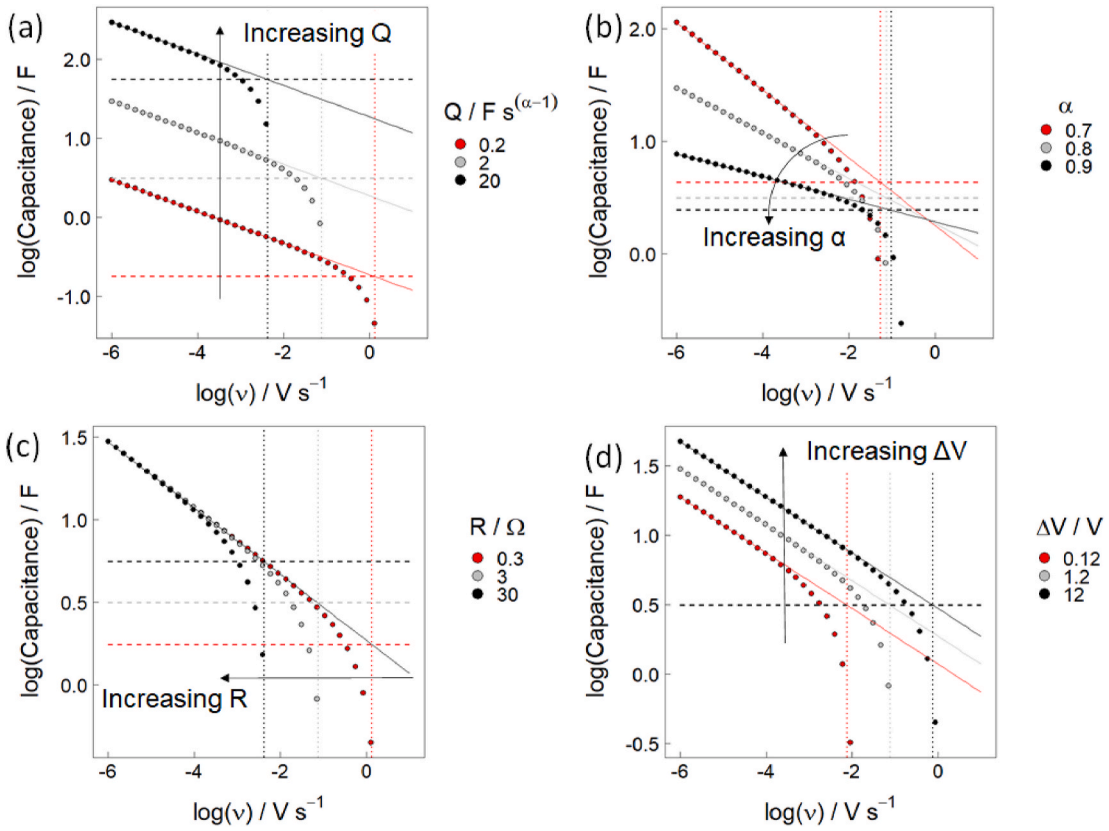

Fig. 3. Results from a simulated R-CPE circuit showing the effective capacitance calculated from Eq. (4) (filled symbols), the capacitance calculated from the Brug formula Eq. (2) (dashed line), the power law in the low-rate region (solid line) and the critical sweep rate (dotted line). The effect of each parameter is shown: Q and ΔV shift the plot along the capacitance axis, α controls the slope of the capacitance, and the critical rate is determined from Q, R, and ΔV. When kept constant, the circuit used in the simulation had Q = 2 F s$^{\alpha-1}$, α = 0.8, R = 3 Ω, and ΔV = 1.2 V.

like" voltammograms and reduced capacitance. The critical rate was found to be

$$\nu_c = \Gamma(3-\alpha)^{\frac{1}{\alpha-1}}(RQ)^{\frac{-1}{\alpha}}\Delta V \tag{10}$$

by equating capacitance in the power law region, Eq. (5), with the capacitance calculated from the Brug formula, Eq. (3). Increasing Q or ΔV shifts the capacitance along the y-axis, and the slope is determined by the value of α. Importantly, R has no impact on the value of capacitance in the low-rate region. Thus, a single CV curve cannot be used to determine R. The only way to determine R from CV would be to experimentally determine the critical rate by taking measurements above and below this rate. This may be possible by placing a resistor of large known resistance in series with the capacitor during CV testing in order to artificially shift the critical rate into a measurable regime.

Since $\nu = \Delta V/t$, Eq. (10) can be used to calculate an effective time constant for the R-CPE,

$$\tau = \Gamma(3-\alpha)^{\frac{1}{\alpha-1}}(RQ)^{\frac{1}{\alpha}} \tag{11}$$

which obeys $\lim_{\alpha\to 1}\tau = e^{\gamma-1}RC \sim 0.66RC$ (γ is the Euler-Mascheroni constant, ~0.577) and $\lim_{\alpha\to 0}\tau = \frac{RC}{2}$. The power law behavior of the capacitance of CPEs also implies that extrapolation to zero frequency [18] is impossible, since the capacitance of the R-CPE system does not exhibit limiting behavior. This means that, even at extremely low rates, CV will not give a sweep rate-independent value of capacitance [8,18] for a system that exhibits CPE behavior. Capacitance is also sometimes extrapolated to infinite frequency [20], which would result in purely resistive behavior and an effectively null capacitance.

The power law trend shown in the simulated R-CPE circuits in Figs. 1–3 is also seen in experimental data. Capacitances taken from the literature calculated using Eq. (4) are shown in Fig. 4 as a function of sweep rate on a log-log scale. This collected data demonstrates that for all types of system (aqueous or non-aqueous, faradaic or non-faradaic), the effective capacitance follows the same power law trend as seen in the simulated R-CPE circuits. Even if individual CV scans reveal obvious redox processes, the capacitance from the integrated current is

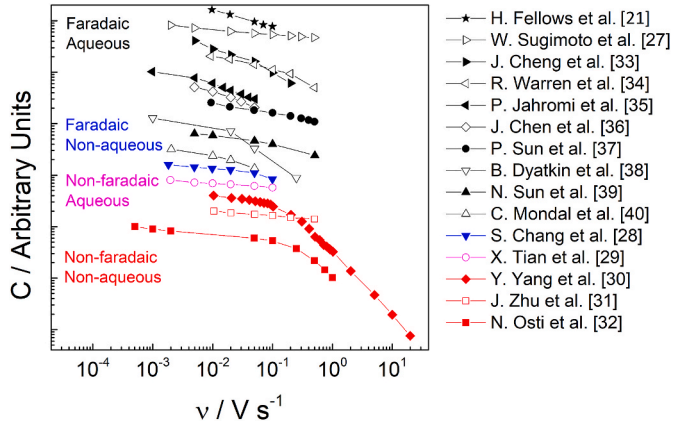

Fig. 4. Literature data showing the power law dependence of capacitance on sweep rate. The power law dependence is seen in aqueous and non-aqueous systems, faradaic and non-faradaic systems, implying that CPE behavior is fundamental to measurements of the double-layer capacitance in electrochemical systems. Capacitances from each source were normalized to the maximum value and then multiplied by a factor to better separate the data [21,27–40].

indistinguishable from that of a simple R-CPE circuit [21]. Power limitations in supercapacitors, i.e. capacitive to resistive switching, have been previously attributed to ionic accessibility of pores in porous electrodes [22,23]. The present work indicates that the power limitations seen in supercapacitors are fundamentally a result of CPE behavior. While diffusive effects in porous structures and pore size distribution have also been used to account for CPE behavior [24,25], whether porosity is the sole or even main cause of the frequency dispersion of CPEs remains to be seen.

The energy and power relationships of EDLCs can now be calculated. Using known equations

$$E = \frac{1}{2} C \Delta V^2 \tag{12}$$

and

$$P = \frac{E}{\Delta t} = \frac{E\nu}{\Delta V} \tag{13}$$

and by inserting Eq. (5) for the capacitance, new equations relating the energy and power of an EDLC to its CPE parameters can be derived as

$$E = \frac{Q \Delta V^{3-\alpha}}{2\Gamma(3-\alpha)} \nu^{\alpha-1} \tag{14}$$

and

$$P = \frac{Q \Delta V^{2-\alpha}}{2\Gamma(3-\alpha)} \nu^{\alpha} \tag{15}$$

together resulting in

$$E = \left(\frac{Q \Delta V^2}{2\Gamma(3-\alpha)} \right)^{\frac{1}{\alpha}} P^{\frac{\alpha-1}{\alpha}} \tag{16}$$

where all parameters have their usual definitions. Note that Eqs. (15-17) were derived based on voltage-controlled charging (CV), meaning that similar but distinct equations are required for galvanostatic charge-discharge (GCD) analysis. Allagui et al. derived an alternative series of equations to calculate the energy stored in a CPE [26], but these equations are expected to be different because the series resistance term is not included.

To compare the classical EIS methods of determining CPE parameters with the CV methods, CPE parameters were calculated in three ways, with example data shown in Fig. 5. In Fig. 5a, individual CV curves were fitted using Eq. (2) to determine Q, α and R. In Fig. 5b, the capacitance calculated from Eq. (4) was plotted as a function of sweep rate and the slope and intercept were used to determine Q and α using Eq. (5). This method was unable to determine R due to lack of data around the critical rate. In Fig. 5c, the low-frequency (<25 Hz) EIS data was fitted to an R-CPE circuit using Eq. (3) as in Refs. [17,41] to determine Q, α, and R. In some devices, the EIS response included semicircles or other sloped lines in the higher-frequency region. While such high-frequency behavior may include very useful information in some cases [42], the following analysis shows that the low-frequency impedance measures the same CPE behavior that determines the CV response.

The results of the different fitting strategies are shown in Fig. 6. The α value calculated from CV, shown in Fig. 6a, is consistently underestimated as compared to the EIS value. Similarly, the value of Q is underestimated in most cases using the CV methods as compared to the EIS method, depicted in Fig. 6b. Nevertheless, the two different CV-based methods give similar results, seen by comparing the open and closed symbols in each figure. The error bars from the fittings using Eq. (6) were determined by taking the average value over the four scan rates in the fitted CV curves. The individual curve fitting was also used to determine R, and the results are shown in Fig. 7. Clearly, the resistance obtained from CV is not close to that determined from the EIS data (note the log scale). Considering the large discrepancy between the CV-fitted R and the EIS value, and the fact that the resistance varies so drastically with sweep rate, the resistance determined from the individual curve fitting cannot be physically realistic. Instead, it is thought to be an artifact of Eq. (2), which approaches $-\infty$ as $V \rightarrow V_i^+$. Lower sweep rates have lower current magnitude at the switching potentials. When the voltammograms at lower rates are fitted with Eq. (2), the lower current magnitude is accounted for in the fitting by increasing resistance. This explains both the larger resistance at rates farther from the critical rate and the power law dependence of the fitted resistance on sweep rate. Eq. (2) can model the current in the quasi-steady-state region properly, which is why Q and α are much less affected by the rate, as shown by the small error bars in Fig. 6.

Capacitance data from supercapacitors of varying CNT aspect ratio were plotted in a dimensionless scale in Fig. 8, where the solid line represents the expectation from Eq. (1). The measured data follows a clear trend, but this is shifted slightly away from the expected value. Simulated circuits verified that the dimensionless method used in Fig. 8 successfully accounts for variation in Q, α, R, and ΔV. Therefore, the discrepancy lies in the value of C_{CV} calculated using Eq. (10) or C_B calculated from Eq. (4). This means that the calculated C_{CV} is either higher than expected, or C_B is lower than expected. The CPE parameters determined from EIS measurements were used to calculate C_B since a value of R is required, and R was unobtainable from the CV data. It can be seen from the results in Fig. 6 that the CPE parameters differ between the two methods, however, the EIS-determined parameters were systematically higher than the CV-determined ones, which should result in a larger than expected value of C_B and a downward, rather than upward, shift in the data presented in Fig. 8. Another possibility is an underlying faradaic reaction in parallel with the CPE behavior. The capacitance from CV was calculated using the forward voltage sweep only, and voltammograms of all devices showed a sharp increase in current at approximately 0.7 V. To reduce the effect of this parallel faradaic

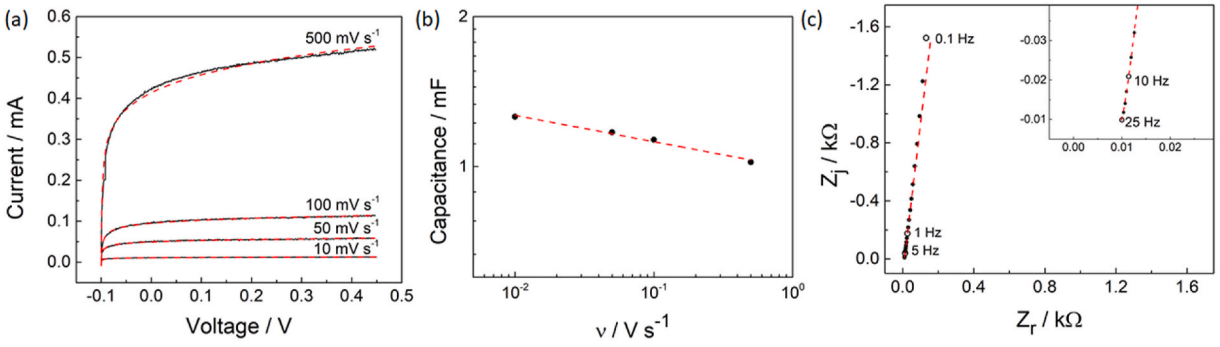

Fig. 5. Experimental data (black) and its fitting (red) for different methods of calculating capacitance and CPE parameters. Individual CV curves can be fit using Eq. (7) (a), the capacitance calculated from Eq. (2) can be fit with a power law (b), and the EIS spectrum can be fit using the equivalent circuit in Eq. (3) (c). (For interpretation of the references to colour in this figure legend, the reader is referred to the Web version of this article.)

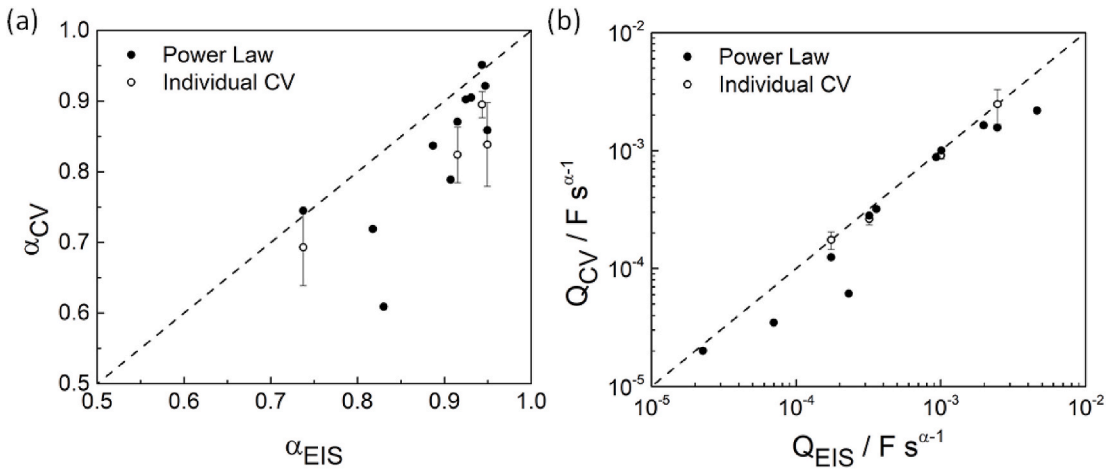

Fig. 6. Comparing α (a) and Q (b) from the different methods for experimental data shows that the two CV methods (individual curve fitting and power law fitting) give comparable results, and that the CV-based methods generally underestimate the CPE parameters compared to EIS. The dashed line shows the desired 1:1 relationship.

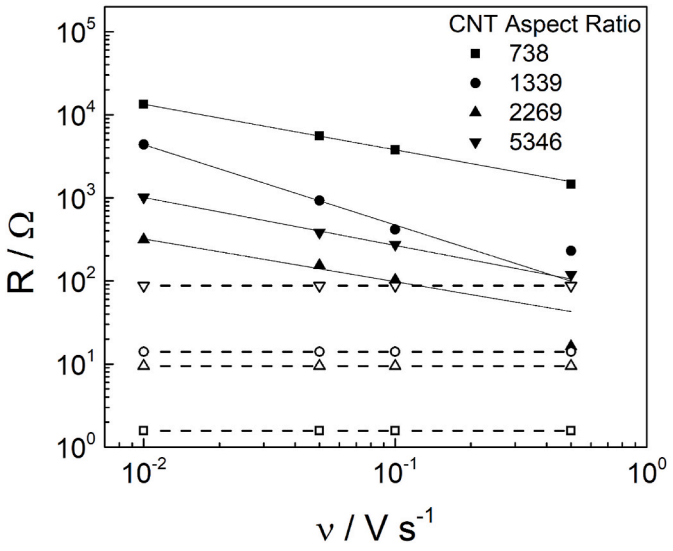

Fig. 7. Resistance determined as a function of sweep rate for selected devices. The dashed line with open symbols indicates the corresponding resistance determined from EIS by the intercept of the low frequency impedance with the Z_r axis.

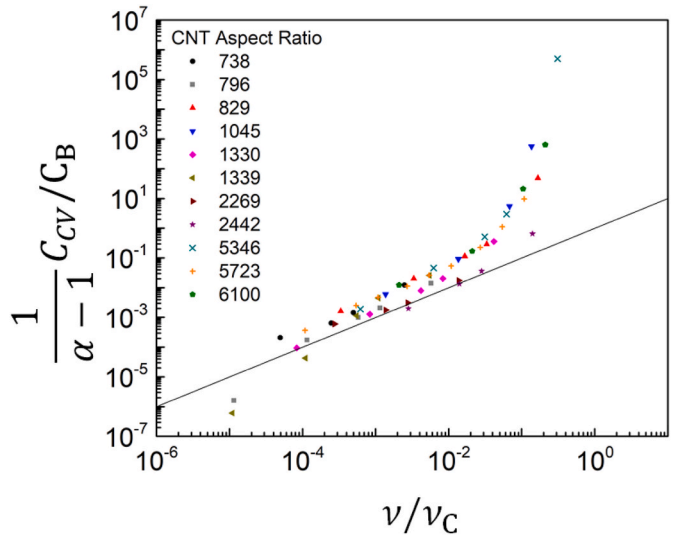

Fig. 8. Experimental data from 11 different carbon nanotube-ionic liquid capacitors plotted as dimensionless capacitance versus dimensionless rate. The solid black line gives the expected relationship based on Eq. (1). The CV rate should be at least two orders of magnitude lower than the critical rate in order to calculate CPE parameters from the capacitance.

response, only the current below 0.5 V was used to calculate the capacitance from CV. The faradaic current passed at this voltage range is expected to be small, but it may have skewed the C_{CV} values higher than expected, resulting in the discrepancy in Fig. 8.

The dimensionless analysis demonstrates that the capacitance from CV only follows the expected trend for rates at least two orders of magnitude lower than the critical rate. As the test rate approaches the critical rate, the data begin to stray significantly from the expected trend. The agreement between the measured data points and the line of expectation in the dimensionless plot indicates that the CPE parameters determined from the low-frequency EIS response are directly related to the integral capacitance of the R-CPE circuit. The data in Fig. 8 also indicates that the high-frequency limit of the impedance is not the most suitable metric of resistance for supercapacitors. In this work, the intercept of the low-frequency arm of the Nyquist plot was used to determine the resistance, rather than the high frequency intercept of the impedance (see Fig. 5c). This value of resistance resulted in good agreement between datasets of CV capacitance. In the dimensionless format used here, changes in R will shift the data along the expected trend, indicating that this lower-frequency resistance is more important in determining the effective performance of supercapacitors than the high frequency intercept of the impedance.

These data can be used to guide future CV experiments of supercapacitors. In order to calculate an accurate value of capacitance, the lowest sweep rate possible should be used, which may be counterintuitive since the current at this low rate will be extremely low. For small capacitances (~1 μF), the noise level at extremely low (<1 mV s^{-1}) rates may obscure measurements. To determine resistance from CV, sweep rates both above and below the critical rate must be measured, and, in an unknown system, that may mean taking many CV scans. For the small time constants encountered in low-capacitance systems, the critical rate may exceed the highest possible sweep rate of many commonly used potentiostats. However, CV may not be necessary at all, since Eq. (5) may be applied using the CPE parameters determined from EIS to predict the entire rate capability of the system below the critical rate. Since EIS can also give the value of R, the critical rate can be determined easily.

This means that a single EIS scan can replace dozens of CV scans. In any case, the CPE parameters of R, Q, and α should be reported in order to make more meaningful comparisons between devices.

In the present work, it has been shown that the power law dependence of capacitance with sweep rate in CV is the result of CPE behavior. The causes of CPE behavior have been an open topic in electrochemistry for decades, and explanations include physical [10] or energetic [43] heterogeneity across the electrode surface, current distribution due to electrode geometry [15,44], pore size distribution [25,45], resistivity distributions within films [46], and more [47–49]. The striking relationship between the CV data and the Brug formula presented in Fig. 8 may provide further evidence that CPE behavior in supercapacitors can generally be thought to arise from a surface distribution of time constants. Further work should be directed at determining a unified theory of CPE behavior.

4. Conclusions

It is well-known that supercapacitors exhibit non-ideal, CPE behavior, and that the capacitance of CPE circuits exhibits a power law dependence on CV sweep rate based on the CPE coefficient α. Until now, this power-law relationship has been analyzed only by relating the slope to the α-value of the CPE, but, in fact, the pre-exponential term has been shown to be directly related to the CPE coefficient Q. The power-law dependence has also been shown to hold only at low sweep rates, at least two orders of magnitude lower than the critical rate determined here. At higher rates, the time constant of the system will suppress the effective capacitance for both high-resistance and high-capacitance systems. It was further found that the capacitance calculated from the Brug formula based on the low-frequency CPE behavior in EIS was directly related to the integral capacitance obtained from CV, and therefore it is proposed that EIS be used in place of CV to report supercapacitor performance. The performance metrics of interest are Q, α, and R, since these determine both the critical rate and the energy-power profile of the device. For the analysis of the resistance, the intercept of the low-frequency CPE arm of the EIS data was shown to determine the effective device performance more so than the high-frequency limit of the impedance. Considering that several CV scans should be taken at each rate to allow the CV response to settle, and that many CV scans must be taken to get an accurate description of the rate capability of a supercapacitor, the time savings available by using the method in the present work are remarkable. It must also be considered that the resistance cannot be determined from CV unless many sweep rates are used, and that the critical rate may not be accessible to many researchers without specialized equipment. This method will allow for faster and easier testing of supercapacitors and more meaningful performance metrics for the comparison and rational design of high-performance supercapacitors.

CRediT authorship contribution statement

Gibson P. Scisco: Conceptualization, Data curation, Formal analysis, Investigation, Methodology, Validation, Visualization, Writing – original draft, Writing – review & editing. **Mark E. Orazem:** Conceptualization, Methodology, Software, Supervision, Validation, Visualization, Writing – review & editing. **Kirk J. Ziegler:** Conceptualization, Funding acquisition, Methodology, Project administration, Resources, Software, Supervision, Validation, Visualization, Writing – review & editing. **Kevin S. Jones:** Conceptualization, Funding acquisition, Methodology, Project administration, Resources, Software, Supervision, Validation, Visualization, Writing – review & editing.

Declaration of competing interest

The authors declare that they have no known competing financial interests or personal relationships that could have appeared to influence the work reported in this paper.

Acknowledgments

The authors would like to thank Mainstream Engineering Corporation for their useful discussions related to this project. This material is based upon work supported by the United States Air Force under Contract No. FA9302-17-C-0001. Any opinions, findings and conclusions or recommendations expressed in this material are those of the author(s) and do not necessarily reflect the views of the United States Air Force. Mark Orazem acknowledges financial support from the University of Florida Foundation Preeminence and the Dr. and Mrs. Frederick C. Edie term professorships. Distribution Statement A. Approved for public release; Distribution is unlimited 412TW-PA-21452.

References

[1] P. Simon, Y. Gogotsi, Materials for electrochemical capacitors, Nat. Mater. 7 (2008) 845–854.
[2] Y. Ge, X. Xie, J. Roscher, R. Holze, Q. Qu, How to measure and report the capacity of electrochemical double layers, supercapacitors, and their electrode materials, J. Solid State Electrochem. 24 (2020) 3215–3230, https://doi.org/10.1007/s10008-020-04804-x.
[3] A. Noori, M.F. El-Kady, M.S. Rahmanifar, R.B. Kaner, M.F. Mousavi, Towards establishing standard performance metrics for batteries, supercapacitors and beyond, Chem. Soc. Rev. 48 (2019) 1272–1341, https://doi.org/10.1039/c8cs00581h.
[4] A. Allagui, A.S. Elwakil, H. Eleuch, Highlighting a common confusion in the computation of capacitance of electrochemical energy storage devices, J. Phys. Chem. C 125 (2021) 9591–9592, https://doi.org/10.1021/acs.jpcc.1c01288.
[5] M.K. Hota, Q. Jiang, Z. Wang, Z.L. Wang, K.N. Salama, H.N. Alshareef, Integration of electrochemical microsupercapacitors with thin film electronics for on-chip energy storage, Adv. Mater. 31 (2019), 1807450, https://doi.org/10.1002/adma.201807450.
[6] M.R. Lukatskaya, S. Kota, Z. Lin, M.Q. Zhao, N. Shpigel, M.D. Levi, J. Halim, P. L. Taberna, M.W. Barsoum, P. Simon, Y. Gogotsi, Ultra-high-rate pseudocapacitive energy storage in two-dimensional transition metal carbides, Nat. Energy. 6 (2017) 1–6, https://doi.org/10.1038/nenergy.2017.105.
[7] A. Sadkowski, Time domain responses of constant phase electrodes, Electrochim. Acta 38 (1993) 2051–2054, https://doi.org/10.1016/0013-4686(93)80339-2.
[8] H. Wang, L. Pilon, Intrinsic limitations of impedance measurements in determining electric double layer capacitances, Electrochim. Acta 63 (2012) 55–63, https://doi.org/10.1016/j.electacta.2011.12.051.
[9] A. Allagui, T.J. Freeborn, A.S. Elwakil, B.J. Maundy, Reevaluation of performance of electric double-layer capacitors from constant-current charge/discharge and cyclic voltammetry, Sci. Rep. 6 (2016), https://doi.org/10.1038/srep38568.
[10] G.J. Brug, A.L.G. van den Eeden, M. Sluyters-Rehbach, J.H. Sluyters, The analysis of electrode impedances complicated by the presence of a constant phase element, J. Electroanal. Chem. 176 (1984) 275–295, https://doi.org/10.1016/S0022-0728(84)80324-1.
[11] C. Montella, LSV/CV modelling of electrochemical reactions with interfacial CPE behaviour, using the generalised Mittag-Leffler function, J. Electroanal. Chem. 667 (2012) 38–47, https://doi.org/10.1016/j.jelechem.2011.12.010.
[12] S. Westerlund, Dead matter has memory, Phys. Scripta 43 (1991) 174–179, https://doi.org/10.1088/0031-8949/43/2/011.
[13] G.P. Scisco, K. Haynes, K.S. Jones, K.J. Ziegler, Single step bonding of thick anodized aluminum oxide templates to silicon wafers for enhanced system-on-a-chip performance, J. Power Sources 474 (2020), https://doi.org/10.1016/j.jpowsour.2020.228643.
[14] W. Watson, M.E. Orazem, EIS: measurement model program, ECSarXiv, 2020, https://doi.org/10.1149/osf.io/kze9x.
[15] K.B. Oldham, The RC time "constant" at a disk electrode, Electrochem. Commun. 6 (2004) 210–214, https://doi.org/10.1016/j.elecom.2003.12.002.
[16] T. Tooming, T. Thomberg, H. Kurig, A. Jänes, E. Lust, High power density supercapacitors based on the carbon dioxide activated d-glucose derived carbon electrodes and 1-ethyl-3-methylimidazolium tetrafluoroborate ionic liquid, J. Power Sources 280 (2015) 667–677, https://doi.org/10.1016/j.jpowsour.2015.01.157.
[17] O. Gharbi, M.T.T. Tran, B. Tribollet, M. Turmine, V. Vivier, Revisiting cyclic voltammetry and electrochemical impedance spectroscopy analysis for capacitance measurements, Electrochim. Acta 343 (2020), https://doi.org/10.1016/j.electacta.2020.136109.
[18] H. Wang, L. Pilon, Physical interpretation of cyclic voltammetry for measuring electric double layer capacitances, Electrochim. Acta 64 (2012) 130–139, https://doi.org/10.1016/j.electacta.2011.12.118.
[19] T.-C. Liu, W.G. Pell, B.E. Conway, S.L. Roberson, Behavior of molybdenum nitrides as materials for electrochemical capacitors: comparison with ruthenium oxide, J. Electrochem. Soc. 145 (1998) 1882–1888, https://doi.org/10.1149/1.1838571.
[20] J.W. Kim, V. Augustyn, B. Dunn, The effect of crystallinity on the rapid pseudocapacitive response of Nb2O5, Adv. Energy Mater. 2 (2012) 141–148, https://doi.org/10.1002/aenm.201100494.

[21] H.M. Fellows, M. Forghani, O. Crosnier, S.W. Donne, Modelling voltametric data from electrochemical capacitors, J. Power Sources 417 (2019) 193–206, https://doi.org/10.1016/j.jpowsour.2018.11.078.
[22] H.D. Yoo, J.H. Jang, J.H. Ryu, Y. Park, S.M. Oh, Impedance analysis of porous carbon electrodes to predict rate capability of electric double-layer capacitors, J. Power Sources 267 (2014) 411–420, https://doi.org/10.1016/j.jpowsour.2014.05.058.
[23] B.E. Conway, W.G. Pell, Power limitations of supercapacitor operation associated with resistance and capacitance distribution in porous electrode devices, J. Power Sources 105 (2002) 169–181, https://doi.org/10.1016/S0378-7753(01)00936-3.
[24] H. Song, Y. Jung, K. Lee, L.H. Dao, Electrochemical impedance spectroscopy of porous electrodes : the effect of pore size distribution, Electrochim. Acta 44 (1999) 3513–3519.
[25] H. Song, H. Hwang, K. Lee, L.H. Dao, The effect of pore size distribution on the frequency dispersion of porous electrodes, Electrochim. Acta 45 (2000) 2241–2257.
[26] M.E. Fouda, A.S. Elwakil, A.G. Radwan, A. Allagui, Power and energy analysis of fractional-order electrical energy storage devices, Energy 111 (2016) 785–792, https://doi.org/10.1016/j.energy.2016.05.104.
[27] W. Sugimoto, T. Kizaki, K. Yokoshima, Y. Murakami, Y. Takasu, Evaluation of the pseudocapacitance in RuO2 with a RuO2/GC thin film electrode, Electrochim. Acta (2004), https://doi.org/10.1016/j.electacta.2003.08.013.
[28] S. Chang, J. Pu, J. Wang, H. Du, Q. Zhou, Z. Liu, C. Zhu, J. Li, H. Zhang, Electrochemical fabrication of monolithic electrodes with core/shell sandwiched transition metal oxide/oxyhydroxide for high-performance energy storage, ACS Appl. Mater. Interfaces 8 (2016) 25888–25895, https://doi.org/10.1021/acsami.6b06073.
[29] X. Tian, H. Ma, Z. Li, S. Yan, L. Ma, F. Yu, G. Wang, X. Guo, Y. Ma, C. Wong, Flute type micropores activated carbon from cotton stalk for high performance supercapacitors, J. Power Sources 359 (2017) 88–96, https://doi.org/10.1016/j.jpowsour.2017.05.054.
[30] Y. Yang, L. He, C. Tang, P. Hu, X. Hong, M. Yan, Y. Dong, X. Tian, Q. Wei, L. Mai, Improved conductivity and capacitance of interdigital carbon microelectrodes through integration with carbon nanotubes for micro-supercapacitors, Nano Res 9 (2016) 2510–2519, https://doi.org/10.1007/s12274-016-1137-3.
[31] J. Zhu, T. Feng, X. Du, J. Wang, J. Hu, L.P. Wei, High performance asymmetric supercapacitor based on polypyrrole/graphene composite and its derived nitrogen-doped carbon nano-sheets, J. Power Sources 346 (2017) 120–127, https://doi.org/10.1016/j.jpowsour.2017.02.034.
[32] N.C. Osti, B. Dyatkin, A. Gallegos, D. Voneshen, J.K. Keum, K. Littrell, P. Zhang, S. Dai, J. Wu, Y. Gogotsi, E. Mamontov, Cation molecular structure affects mobility and transport of electrolytes in porous carbons, J. Electrochem. Soc. 166 (2019), https://doi.org/10.1149/2.0131904jes. A507–A514.
[33] J. Cheng, B. Zhao, W. Zhang, F. Shi, G. Zheng, D. Zhang, J. Yang, High-performance supercapacitor applications of NiO-Nanoparticle-Decorated millimeter-long vertically aligned carbon nanotube Arrays via an effective supercritical CO 2 -assisted method, Adv. Funct. Mater. 25 (2015) 7381–7391, https://doi.org/10.1002/adfm.201502711.
[34] R. Warren, F. Sammoura, F. Tounsi, M. Sanghadasa, L. Lin, Highly active ruthenium oxide coating via ALD and electrochemical activation in supercapacitor applications, J. Mater. Chem. A. 3 (2015) 15568–15575, https://doi.org/10.1039/c5ta03742e.
[35] S. Pilban Jahromi, A. Pandikumar, B.T. Goh, Y.S. Lim, W.J. Basirun, H.N. Lim, N. M. Huang, Influence of particle size on performance of a nickel oxide nanoparticle-based supercapacitor, RSC Adv. 5 (2015) 14010–14019, https://doi.org/10.1039/C4RA16776G.
[36] J. Chen, J. Xu, S. Zhou, N. Zhao, C.P. Wong, Amorphous nanostructured FeOOH and Co-Ni double hydroxides for high-performance aqueous asymmetric supercapacitors, Nano Energy 21 (2016) 145–153, https://doi.org/10.1016/j.nanoen.2015.12.029.
[37] P. Sun, H. Yi, T. Peng, Y. Jing, R. Wang, H. Wang, X. Wang, Ultrathin MnO2 nanoflakes deposited on carbon nanotube networks for symmetrical supercapacitors with enhanced performance, J. Power Sources 341 (2017) 27–35, https://doi.org/10.1016/j.jpowsour.2016.11.112.
[38] B. Dyatkin, Y. Zhang, E. Mamontov, A.I. Kolesnikov, Y. Cheng, H.M. Meyer, P. T. Cummings, Y. Gogotsi, Influence of surface oxidation on ion dynamics and capacitance in porous and nonporous carbon electrodes, J. Phys. Chem. C (2016), https://doi.org/10.1021/acs.jpcc.6b01204.
[39] N. Sun, D. Zhou, W. Liu, A. Li, Y. Su, P. Jiang, Y. Zou, S. Shi, F. Liu, Sputtered titanium nitride films with finely tailored surface activity and porosity for high performance on-chip micro-supercapacitors, J. Power Sources 489 (2021), 229406, https://doi.org/10.1016/j.jpowsour.2020.229406.
[40] C. Mondal, D. Ghosh, T. Aditya, A.K. Sasmal, T. Pal, Mn_3O_4 nanoparticles anchored to multiwall carbon nanotubes: a distinctive synergism for high-performance supercapacitors, New J. Chem. (2015), https://doi.org/10.1039/C5NJ00825E.
[41] A. Allagui, M.E. Fouda, Inverse problem of reconstructing the capacitance of electric double-layer capacitors, Electrochim. Acta 390 (2021), 138848, https://doi.org/10.1016/j.electacta.2021.138848.
[42] G.P. Scisco, M.E. Orazem, K.J. Ziegler, K.S. Jones, Resistivity of mesopore-confined ionic liquid determined by electrochemical impedance spectroscopy, Electrochim. Acta 378 (2021), 138112, https://doi.org/10.1016/j.electacta.2021.138112.
[43] Z. Kerner, T. Pajkossy, On the origin of capacitance dispersion of rough electrodes, Electrochim. Acta 46 (2000) 207–211, https://doi.org/10.1016/S0013-4686(00)00574-0.
[44] C.L. Alexander, B. Tribollet, M.E. Orazem, Contribution of surface distributions to constant-phase-element (CPE) behavior: 1. Influence of roughness, Electrochim. Acta 173 (2015) 416–424, https://doi.org/10.1016/j.electacta.2015.05.010.
[45] M. Musiani, M. Orazem, B. Tribollet, V. Vivier, Impedance of blocking electrodes having parallel cylindrical pores with distributed radii, in: Electrochim. Acta, 2011, https://doi.org/10.1016/j.electacta.2010.12.004.
[46] B. Hirschorn, M.E. Orazem, B. Tribollet, V. Vivier, I. Frateur, M. Musiani, Constant-phase-element behavior caused by resistivity distributions in films, I. Theory, J. Electrochem. Soc. 157 (2010) C452–C457, https://doi.org/10.1149/1.3499564.
[47] C.L. Alexander, B. Tribollet, V. Vivier, M.E. Orazem, Contribution of surface distributions to constant-phase-element (CPE) behavior: 3. Adsorbed intermediates, Electrochim. Acta 251 (2017) 99–108, https://doi.org/10.1016/j.electacta.2017.08.081.
[48] S.M. Rezaei Niya, M. Hoorfar, On a possible physical origin of the constant phase element, Electrochim. Acta 188 (2016) 98–102, https://doi.org/10.1016/j.electacta.2015.11.142.
[49] S. Erol, M.E. Orazem, The influence of anomalous diffusion on the impedance response of LiCoO2|C batteries, J. Power Sources 293 (2015) 57–64, https://doi.org/10.1016/j.jpowsour.2015.05.047.